SCIENCE CHINA
Technological Sciences

•Article•

November 2021 Vol.64 No.11: 2427–2440
https://doi.org/10.1007/s11431-021-1880-1

Structured road-oriented motion planning and tracking framework for active collision avoidance of autonomous vehicles

ZHANG ZiWei[1], ZHENG Ling[1,2*], LI YiNong[1,2], ZENG PengYun[3] & LIANG YiXiao[1]

[1] *College of Mechanical and Vehicle Engineering, Chongqing University, Chongqing 400030, China;*
[2] *State Key Laboratory of Mechanical Transmissions, Chongqing University, Chongqing 400044, China;*
[3] *Macro Net Communication Co., Ltd., Chongqing 400000, China*

Received March 25, 2021; accepted June 22, 2021; published online September 27, 2021

This paper proposes a novel motion planning and tracking framework based on improved artificial potential fields (APFs) and a lane change strategy to enhance the performance of the active collision avoidance systems of autonomous vehicles on structured roads. First, an improved APF-based hazard evaluation module, which is inspired by discrete optimization, is established to describe driving hazards in the Frenet-Serret coordinate. Next, a strategy for changing lane is developed in accordance with the characteristics of the gradient descent method (GDM). On the basis of the potential energy distribution of the target obstacle and road boundaries, GDM is utilized to generate the path for changing lane. In consideration of the safety threats of traffic participants, the effects of other obstacles on safety are taken as additional safety constraints when the lane-changing speed profile for ego vehicles is designed. Then, after being mapped into the Cartesian coordinate, the feasible trajectory is sent to the tracking layer, where a proportional-integral control and model predictive control (PI-MPC) based coordinated controller is applied. Lastly, several cases composed of different road geometrics and obstacles are tested to validate the effectiveness of the proposed algorithm. Results illustrate that the proposed algorithm can achieve active collision avoidance in complex traffic scenarios.

autonomous vehicles, motion planning, structured road, artificial potential fields, collision avoidance

Citation: Zhang Z W, Zheng L, Li Y N, et al. Structured road-oriented motion planning and tracking framework for active collision avoidance of autonomous vehicles. Sci China Tech Sci, 2021, 64: 2427–2440, https://doi.org/10.1007/s11431-021-1880-1

1 Introduction

Vehicles are beneficial to the daily life of humans. However, many traffic accidents have resulted in thousands of injuries and deaths. Autonomous vehicle (AV) technologies provide efficient ways to alleviate or even solve the above problem because these technologies can take appropriate measures to handle emergency situations. In recent decades, advanced driving assistance systems, such as autonomous emergency braking [1], adaptive cruise control [2,3], auto parking assistance, and lane-keeping assistance, have equipped some passenger cars, thereby providing a potential and solid basis for highly automatic driving technologies.

In accordance with relevant data about AVs, many versions for testing or production have already been successfully developed; examples include Baidu Apollo, Google car, and Tesla, which mainly consist of perception, decision-making, and control layers. For a detailed explanation of each layer, please refer to ref. [4]. This paper mainly focuses on the layers of decision-making and tracking.

The decision-making layer commonly consists of global route planning, motion planning, and local trajectory planning. Route planner aims to obtain the optimal route to satisfy drivers' demands [5] (travel efficiency or fuel-saving). Subsequently, considering traffic information, motion planning decides proper driving maneuvers (overtaking or car

*Corresponding author (email: zling@cqu.edu.cn)

following) along the decided route. Then, a safe, comfortable, and efficient trajectory based on the appointed driving tasks is obtained by the lowest planner.

Local path planning methods can be classified into four categories [6]: graph search-based method, sampling-based method, interpolating curve method, and numerical optimization-based method. In the graph search-based method, the driving environment is discretized into a map, which is full of grids or lattices; ego vehicles and obstacles occupy the elements in the map. Then, a safe path could be obtained by map searching methods, including Djikstra, A*, and state lattice algorithm. In the early years, Djikstra was developed and had shown outstanding performance in the DARPA challenge by searching the single-source shortest path [7,8]. The A* algorithm, which is extended from Djikstra, was also applied in Team Stanford's Junior [9]. Although these methods are effective, the path is discontinuous, and vehicle dynamics are not considered and thus may result in jerk and failing to track. To solve this demerit, a high-dimensional state lattice is constructed by adding velocity, heading angle, and other kinematics information to elements, and a smooth path is obtained via a lookup table [10,11]. However, the computational burden is heavy due to traversing all elements. Sampling-based methods, such as the probabilistic roadmap method [12] and the rapidly exploring random tree [13], have gained much interest due to their capability of fast planning in nonholonomic constraints. The interpolating curve method benefits from the products of the smooth path through clothoid curves [14], Bézier curves [15,16], and other kinds of spline curves [17,18]. However, to make the planned path smoother and more continuous, more control points or higher curve degrees are required, thus increasing the computational burden. Numerical optimization-based methods, including discrete optimization, artificial potential field (APF)-based method, and optimal control algorithm, have been widely used due to their logic and global and optimal consideration for potential paths. Ziegler et al. [19] proposed an optimal path planner to obtain a continuous and optimal path with the objective function of minimizing lateral offset, acceleration, and jerk. Accuracy could be enhanced by increasing the number of candidate paths, but the computational burden is also increased. In ref. [20], the virtual elastic band and Newton–Raphson algorithm were utilized to design a path to avoid obstacles based on the force equilibrium. By modifying the functions of APFs, Ji et al. [21] established a novel path planning system that could fast plan the collision avoidance path. Hang et al. [22] proposed a game-based motion planning algorithm that considers social intervehicle behaviors described by the APFs. In this manner, the planner enables proper decision-making for AVs to handle traffic scenarios that exist social interactions with other traffic participates and reflect real traffic environment more exactly. Based on the Lagrangian operator, Li et al. [23] presented an integrated dynamic controller for wheeled mobile robots and well mediated the contradictory demands between collision avoidance and tracking accuracy. Additionally, in refs. [24,25], the ego vehicle can directly respond to driving environments with appropriate maneuvers by an integrated model predictive controller. However, given the fusion of the planning and control layers, the framework of the algorithm is complex, thus limiting its practical applications.

The aim of tracking control is to control paths along a predefined trajectory with simultaneously satisfying stability demands [26]. Han et al. [27] developed an adaptive PID controller for tracking lateral paths in which the PID controller parameters are tuned by a neural network. Wang et al. [28] established a kind of output-feedback triple-step controller, which could realize coordinated control for the vehicle without measuring lateral velocity. Ji et al. [29] proposed a shared control paradigm-based controller in which Stackelberg game theory is applied to make an active front steering system and active rear steering system and thereby provide additional stability for path tracking control. As the extension of optimal control, model predictive control (MPC) is also a widely used approach in the field of motion tracking control. Ren et al. [30] formulated an MPC problem to compute steering angles and total desired driving/braking force, and then the total force is distributed to each wheel optimally by a sliding model controller. Guo et al. [31] designed feasible envelopes in accordance with road boundaries and vehicle shape as driving safety constraints for an MPC controller. Varied sample time and prediction horizons are also used to address modeling error to guarantee the performance of path following further.

In summary, the aforementioned methods provide good results. However, almost all previous APF-based approaches have weak practicality, which could only be adopted in simple traffic scenarios. First, given the influences of obstacles' potential coupling areas, collision-free paths may be singular or even unsolvable (trapped in local minimum) in multi-obstacle cases. Second, the planned overtaking process [20] is too long, thus reducing traffic efficiency and degrading driving safety. Moreover, these approaches cannot cope with traffic situations for various road geometries because existing APF-based danger evaluation models that are described in the Cartesian coordinate are only applicable for straight roads. Thus, to advance the performance of planning systems, this paper presents a novel motion planning and tracking framework for the collision avoidance of AVs. The structure of the entire system, which has two parts, is illustrated in Figure 1. First, the planning layer generates the desired motion. Second, the tracking control layer tracks planned trajectories. According to perception information, the improved danger evaluation model, which is in the Frenet-Serret coordinate, generates the hazard distribution of the driving environment and provides a safety basis for path

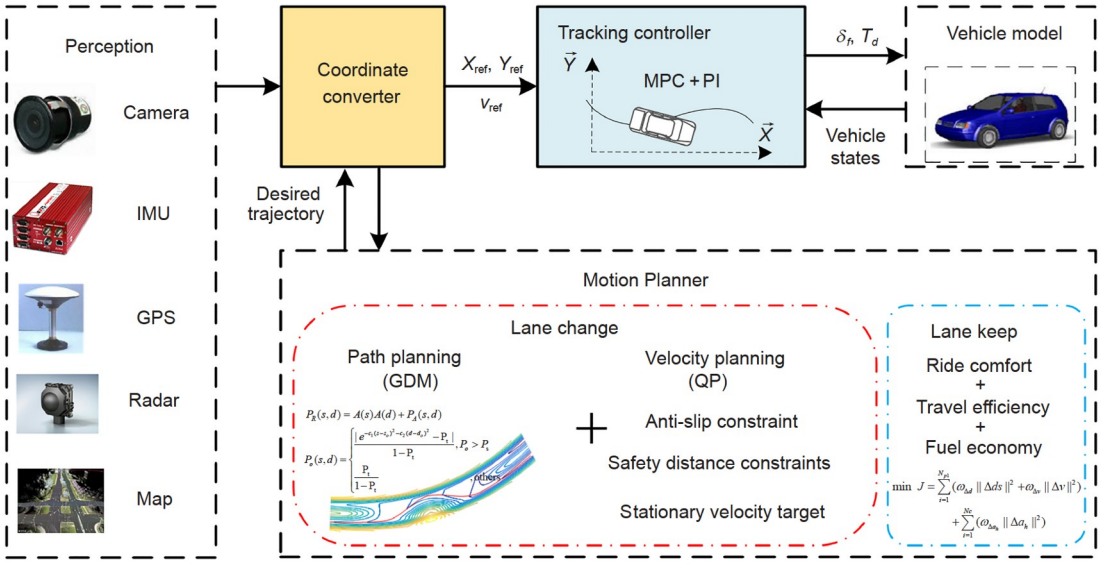

Figure 1 (Color online) Overall structure of the collision avoidance system.

planning. Then, on the basis of the characteristics of the GDM, the path planning problem for collision avoidance in complex dynamic scenes is simplified into a single static target obstacle (TO) avoidance problem. Lane change path is generated by GDM in accordance with the potential energy distribution of TO and road boundaries. Moreover, extra safety distance constraints considering other obstacles are introduced into velocity planning to ensure dynamic security. Thus, potential safety threats are fully considered. Once the lane change path is determined, it would not change until it is finished. The real-time velocity update also ensures the driving security during the lane-changing process. For the control layer, the path following task is appointed to different controllers according to movement directions. The lateral path tracking problem is transferred to a standard quadratic programming problem and solved by sequential quadratic programming, which can balance tracking accuracy and computational burden. In addition, given the difference of coordinate framework in two layers [32], a coordinate converter is constructed to ensure the accuracy of information transmission among different layers.

The main contributions of this paper are as follows: (Ⅰ) An improved APF-based hazard evaluation module is developed to describe the driving hazard in the Frenet-Serret coordinate framework through leveraging coordinate transformation, which is inspired by the discrete optimization method. The hazard evaluation module has good adaptability and applicability, which can be directly utilized for different road geometrics rather than modifying the potential functions (PFs) according to the road geometrics. (Ⅱ) A lane change strategy is designed to deal with the demerits of GDM's application in complex traffic environments. By hierarchically considering potential collision threats of other traffic participates, the algorithm can well address the problems of singularity and insolubility and prevent step changes between different cycles. Thus, smooth and reasonable collision-free trajectories can be obtained in complex traffic scenes.

The remainder of this paper is organized as follows: The main elements of the planning algorithm, including improved APFs and strategy for changing lane, are explained in detail in Section 2. Section 3 develops a coordinated tracking controller. Simulation results are presented in Section 4. Lastly, a brief conclusion is given in Section 5.

2 Motion planning algorithm

This section focuses on designing the motion planning algorithm. First, the method for mapping points between the Cartesian and Frenet-Serret coordinates is introduced. Next, the improved PFs for obstacles and road lane markers are defined. Lastly, a motion planning strategy is proposed in accordance with the characteristics of GDM.

To simplify the derivation of a collision-free trajectory, two assumptions used in this paper are as follows.

(1) The waypoints of the centerline could be obtained from the vehicle networking or high-precision map in advance.

(2) The perception layer is absolutely reliable and accurate in real-time without noise and delay.

2.1 Coordinate transformation

To evaluate the hazard of the driving environment in a unified framework, a fixed earth coordinate system is essential to the safety system. Most path planning research based on

APFs is developed in the Cartesian coordinate, which is convenient for straight-road scenarios. However, evaluating hazards for nonstraight ones becomes much complex that different geometric parts require different modified PFs rather than the same formulations. Nevertheless, the heavy modification task can be omitted when evaluating hazards in the Frenet-Serret coordinate. Regardless of the kind of geometric, the road can always be treated as a "straight road" in the Frenet-Serret coordinate, and so can the discrete optimization [33]. Therefore, in contrast to previous research [21,34,35], the PFs in this paper are modified into a curvilinear coordinate frame (s, d), which makes the algorithm more practical and enhances the adaptability to road geometries. Here, s is the arc length vector along the reference lane's centerline, and d is the normal offset vector from the reference lane's centerline.

In accordance with the sequence of waypoints obtained in advance, the reference centerline of the road (x_c, y_c) can be parameterized into a cubic polynomial spline [33,36].

$$\begin{cases} x_c(s) = a_0 + a_1 s + a_2 s^2 + a_3 s^3, \\ y_c(s) = b_0 + b_1 s + b_2 s^2 + b_3 s^3, \end{cases} \tag{1}$$

where s is the arc length. (a_0, a_1, a_2, a_3, b_0, b_1, b_2, b_3) represent the fitting parameters of the road. Other points can be mapped into the Frenet-Serret coordinate according to (x_c, y_c) via the orthogonal vector method. As shown in Figure 2, $P_1(x_1, y_1)$ is an arbitrary point, which is not on the reference centerline, and P_{0i} (i=1, 2, …, n) are the points on the reference centerline whose Frenet-Serret and Cartesian coordinates are (s_i, 0) and (x_{ci}, y_{ci}), respectively. The vector of the line connecting P_1 with P_{0i} is $\mathbf{P_1P_{0i}}$, and the tangent vector of the centerline at point P_{0i} is ($x_{ci}(s)'$, $y_{ci}(s)'$). It can always find a corresponding point P_{0r} on the reference centerline, whose normal vector is the vector $\mathbf{P_1P_{0r}}$. $|\mathbf{P_1P_{0r}}|$ is the shortest distance between P_1 and the reference centerline. Therefore, the Frenet-Serret coordinate of P_1 is (s_r, $|\boldsymbol{P_1P_{0r}}|$).

By contrast, given the control algorithm established in the Cartesian coordinate, the generated planning results should be remapped into the Cartesian coordinate before conveying to the tracking layer. In accordance with the corresponding point on the reference centerline (x_{cr}, y_{cr}), other edges of the road (x_1, y_1), which are not on the reference centerline, can be obtained.

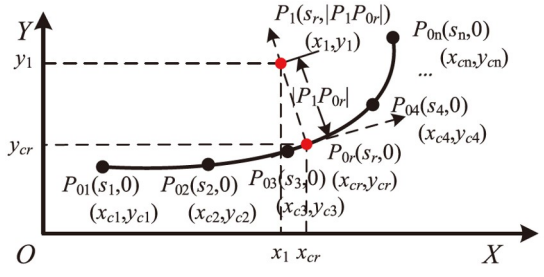

Figure 2 (Color online) Geometric relationship between an arbitrary point and the centerline.

$$\begin{cases} x_1(s) = x_{cr}(s) - d\sin(\theta), \\ y_1(s) = y_{cr}(s) + d\cos(\theta), \end{cases} \tag{2}$$

where d=$|\mathbf{P_1P_{0r}}|$ is the normal offset from the reference centerline. θ denotes the heading angle of the reference road's centerline, and its mathematical expression is formulated as

$$\theta = \arctan\left(\frac{y'_{cr}(s)}{x'_{cr}(s)}\right). \tag{3}$$

Therefore, (x_1, y_1) can be obtained from eqs. (2) and (3).

$$\begin{cases} x_1(s) = x_{cr}(s) - d\dfrac{y'_{cr}(s)}{\sqrt{\left(x'_{cr}(s)\right)^2 + \left(y'_{cr}(s)\right)^2}}, \\ y_1(s) = y_{cr}(s) + d\dfrac{x'_{cr}(s)}{\sqrt{\left(x'_{cr}(s)\right)^2 + \left(y'_{cr}(s)\right)^2}}. \end{cases} \tag{4}$$

2.2 Danger evaluation based on artificial potential fields

The universal hazard potential energy mainly consists of road potential energy and the obstacle potential energy.

$$P_U(s,d) = P_R(s,d) + P_O(s,d), \tag{5}$$

where P_U denotes the universal potential energy; P_R and P_O represent the potential energy of road and obstacle, respectively.

The PFs of the road are the key components of the APFs because they ensure ego vehicle run within the road boundaries and move along the centerline of the target lane without any obstacles ahead. The PFs of the road are expressed as

$$P_R(s,d) = A(s)A(d) + P_A(s,d), \tag{6}$$

where $P_A(s, d)$ represents the attractive PF of the target point, which mainly attracts ego vehicles to move to the desired point. $A(s)$, $A(d)$ denote the amplitude roads' repulsive potential energy in the S-axis and D-axis direction, and their mathematical expressions can be written as

$$A(d) = \left(\frac{[|\,sgn(d-D_l) + sgn(d-D_r)\,|(1-P_m)]}{4} + \frac{P_m}{2}\right) \times\left[\cos\left(\frac{2\pi(d+0.5Lw)}{Lw}\right) + 1\right], \tag{7}$$

$$A(s) = \begin{cases} 0, & 0 \le |\,s - s_o\,| < S_d, \\ \dfrac{|s-s_o| - S_d}{S_t - S_d}, & S_d \le |\,s - s_o\,| < S_t, \\ 1, & S_t \le |\,s - s_o\,|, \end{cases} \tag{8}$$

$$P_A = \frac{|d - D_r| + |\,s - s_o - 0.5S_s|}{100}, \tag{9}$$

where P_{m} is the potential energy of the road's middle line, which plays a crucial role in preventing ego vehicles from unnecessary lane-change maneuvers. L_w is the lane width. D_r and D_l are the normal offsets of the right and left lanes from the reference centerline, respectively. (s_o, d_o) is the position of the obstacle. S_t and S_s denote the range of the repulsive and universal PFs in the S-axis direction (S_t is always wider than S_d). S_d is the driver-desired intervehicle distance, which is determined by the speed of the ego vehicle; it can be formulated as

$$S_d = t_h v_h + d_0, \tag{10}$$

where t_h is the nominal time headway, v_h denotes the speed of the ego vehicle, and d_0 is the stillstand distance.

The repulsive PF primarily makes ego vehicles keep a safe distance from obstacles. On the basis of relative kinematic information, a modified two-dimensional Gaussian function is introduced to describe the collision risk. When an ego vehicle goes toward obstacles, the repulsive potential energy jumps, thus pushing the ego vehicle to change lane and avoid a collision. The repulsive PF is constructed as

$$P_o(s,d) = \begin{cases} \dfrac{\left| e^{-c_1(s-s_o)^2 - c_2(d-d_o)^2} - P_t \right|}{1-P_t}, & P_o > P_{\mathrm{s}}, \\ \dfrac{P_t}{1-P_t}, & \text{others}, \end{cases} \tag{11}$$

where P_t and $P_s = P_t/(1-P_t)$ are the thresholds of the repulsive PF. c_1 and c_2 are the standard deviation of the repulsive field in the S-axis and D-axis directions, respectively; they determine the range and the shape of the fields. Figure 3 shows the hazard map of the entire structured road at a moment. And it should be noted that hazard evaluation by improved APFs agrees with those obtained by original ones in traffic scenarios where two versions of evaluation approaches can be utilized directly.

2.3 Hierarchical motion planning for collision avoidance

As aforementioned, the dangerous potential energy distribution of the driving environment is described by the trigonometric function and the two-dimensional modified Gaussian function, which provides a precise basis for the local path design. In this paper, GDM is applied to plan a safe path for the ego vehicle by searching the direction of the fastest potential energy descent. The negative gradient of universal energy with respect to distance in different directions are the induced forces of the ego vehicle at the current moment, and the forces are formulated as eqs. (12) and (13).

$$\mathbf{F}_t = \sqrt{\mathbf{F}_s^2 + \mathbf{F}_\mathbf{d}^2}, \tag{12}$$

$$[\mathbf{F_s}, \mathbf{F_d}] = -\left[\frac{\partial P_{\mathrm{R}}}{\partial s} + \frac{\partial P_o}{\partial s}, \frac{\partial P_{\mathrm{R}}}{\partial d} + \frac{\partial P_o}{\partial d}\right], \tag{13}$$

where $\mathbf{F}_t$ is the total induced force of the APFs. $\mathbf{F_s}$ and $\mathbf{F_d}$ denote the induced forces in the S, D direction of the APFs, respectively. Following the induced forces, the ego vehicle could always move toward the direction where the driving risk drops fast. In accordance with the position (s_k, d_k) and the total induced force at the current step, the position (s_{k+1}, d_{k+1}) for the next step of the ego vehicle can be obtained.

$$\begin{cases} s_{k+1} = s_k + \gamma \dfrac{\| \mathbf{F_s} \|}{\| \mathbf{F_t} \|}, \\ d_{k+1} = d_k + \gamma \dfrac{\| \mathbf{F_d} \|}{\| \mathbf{F_t} \|}, \end{cases} \tag{14}$$

where γ is the step length of each planning step. However, the performance of GDM relies considerably on the energy distribution, so it can only handle simple and static traffic scenarios. When GDM encounters multiple obstacles or complex scenarios, it is easily trapped into the local minimum or plans a strange-shaped path due to the coupling potential energy of different obstacles, as shown in Figure 4 (a) and (b). In addition, given the change of energy distribution and the ego vehicle position, step changes always exist between different planning cycles. These changes become huge during the lane-changing process at high speed, resulting in a path curvature that is too large to satisfy vehicle dynamics, as shown in Figure 4(c). Therefore, conventional GDM cannot perfectly cope with actual traffic scenarios, that is, any obstacle combinations of numbers and styles. However, the planning results of GDM are smooth and continuous only when handling single static obstacle scenarios.

Thus, a lane change strategy is proposed to overcome or avoid these shortcomings based on the characteristics of GDM. The core idea of the algorithm is to convert complex traffic scenes into single static obstacle collision avoidance scenes on the premise of driving safety. That is, a lane change path is first generated by GDM, assuming a TO on the road; then, the velocity planner considers other obstacles and safety constraints. Moreover, once the vehicle changes lane, the planned path would not change until the lane change process is finished, and the dynamic security of the whole process is managed by real-time velocity updates. Therefore, the planning problem is transformed into a single static obstacle collision avoidance problem because the lane change path is only associated with the position of TO at starting point of changing lane. Thus, the reasonable and smooth path

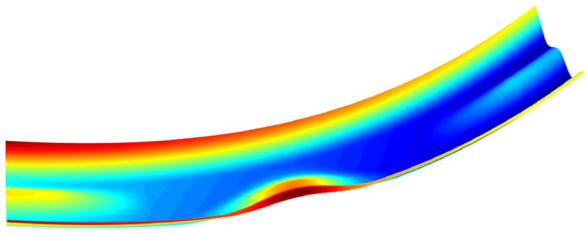

Figure 3 (Color online) Hazard map of a driving environment.

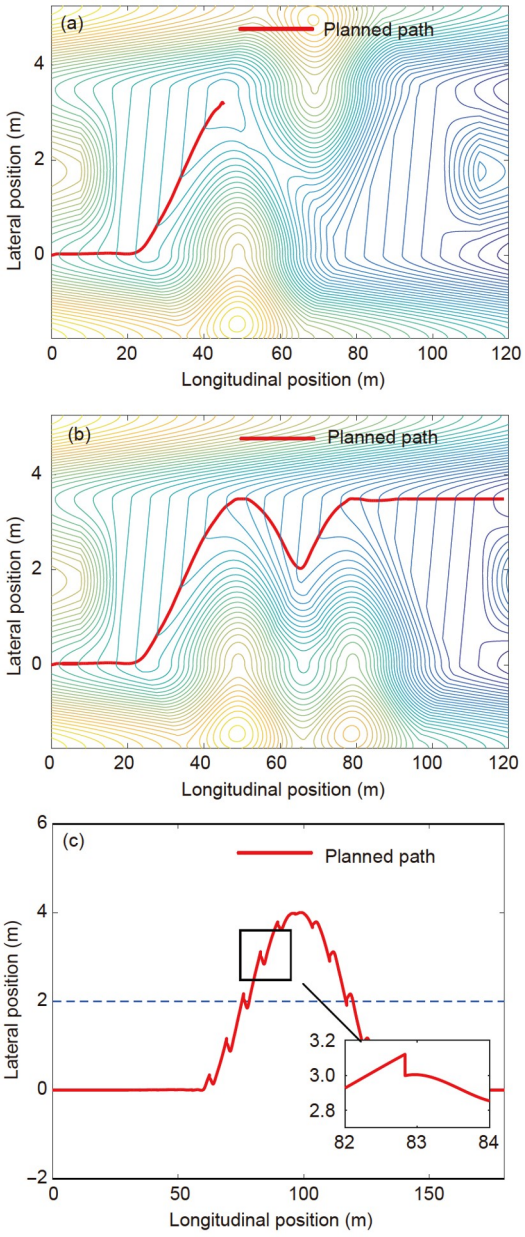

Figure 4 (Color online) (a) Results trapped in the local minimum, (b) strange-shaped results, and (c) unsmooth results when encountering moving obstacles.

is generated by the aforementioned scene transformation and hierarchically considering driving security. The overall logic of strategy is shown in Figure 5.

First, whether or not the ego vehicle is in the lane change process at the current moment is judged, i.e., judging whether or not the change flag is 1. If the ego vehicle is not in the lane change process, the whole process of planning trajectory needs to be performed; otherwise, the next planning cycle enters velocity planning directly to adjust the speed for lane changing and guarantee dynamic safety. After the change flag judgment, the planner picks out TO according to the obstacles' position and judges whether or not TO is within

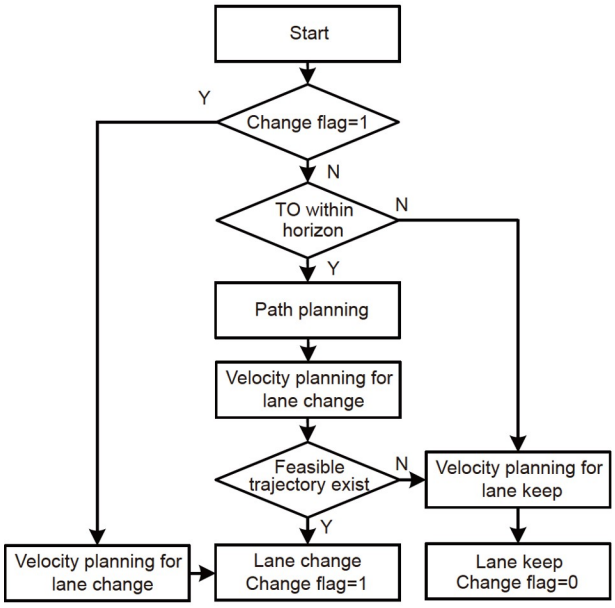

Figure 5 Logic of lane change strategy.

the preset horizon D_t (TO is a slow obstacle that is the nearest to the ego vehicle at the same lane). If TO is within the horizon, it enters the module of path planning for changing lane; otherwise, the ego vehicle would keep the current lane, and the change flag is still 0. In the planner, the path for lane changing is generated by GDM according to the energy distributions of the road and TO. Given that other obstacles are neglected during the path planning process, the velocity planner considers safety distance constraints to ensure dynamic safety after obtaining a path for changing lane. If a feasible trajectory can be obtained, then the ego vehicle sets about to change lane, and the change flag is set to 1; otherwise, the ego vehicle would keep the current lane to wait for overtaking, and the change flag is still 0.

(1) Velocity planning for lane change

After path generation, the speed profile is designed in accordance with the planned path to ensure that the trajectory is feasible and secure. Given the differences in road conditions, the threshold value of the tire forces also varies. To ensure vehicle stability, lateral acceleration must be limited within a threshold. When a vehicle turns in a steady state, its centripetal force is provided completely by the lateral tire forces, and the expression can be formulated as

$$ma_y = \frac{mv_h^2}{R} \le \mu mg, \tag{15}$$

where a_y is the lateral acceleration; μ denotes the adhesion coefficients; R represents the minimal steering radius, and its reciprocal is the curvature of the path, i.e., $R=1/\kappa$. The curvature $\kappa(s)$ of each point on the path can be calculated from the generated path. Therefore, the antislip constraint along the path could be determined.

$$v_h(s) \le \min\left(\sqrt{\frac{a_{y\max}}{\kappa(s)}}\right) = \min\left(\sqrt{\frac{\mu g}{\kappa(s)}}\right). \tag{16}$$

Furthermore, the velocity planner should strive to keep the velocity of the ego vehicle stable and constant to make the lane-changing process comfortable; thus, the objective functison of velocity planning during the lane change can be formulated as

$$J = \sum_{k=1}^{N_p}(\omega_v \parallel v_h(t+k \mid t) - v_o \parallel^2 + \omega_{\Delta a} \parallel \Delta a(t+k \mid t) \parallel^2), \tag{17}$$

where v_h and Δa are the velocity and acceleration increments of the ego vehicle, respectively; v_0 is the initial lane-change speed of the ego vehicle; $N_p = S_p(k)/v(k)$ is the predictive step; S_p is the length of the planned path; ω_v, $\omega_{\Delta a}$ are the corresponding weights.

Only the hazard energy distribution of TO is used in path planning; thus, the safety constraints of equivalent relative distance are added to make ego vehicles keep a safe distance from other obstacles to prevent collision with them. The formulation is expressed as

$$S_e < |\Delta s_{ei}(t+k \mid t)|, \tag{18}$$

where S_e is the desired equivalent safety distance, and $\Delta s_{ei}(t+k|t)$ is the relative distance between the ego vehicle and other obstacles in the S-axis direction at the k-th prediction interval. S_e is equal to S_d, and $\Delta S_{ei}(t+k|t)$ can be formulated as

$$\left|s_e(t+k \mid t) - s_{oi}(t+k \mid t)\right| = \left|\Delta s_{ei}(t+k \mid t)\right|, \tag{19}$$

where $s_e(t+k|t)$ denotes the position of the ego vehicle in the S-axis direction at the k-th prediction interval, and $s_{oi}(t+k|t)$ represents the S coordinate of other obstacles at the k-th prediction interval. Therefore, the velocity planning problem is written as

$$\begin{aligned} \min:\ & J = \sum_{k=1}^{N_p}(\omega_v \left\| v_h(t+k \mid t) - v_o \right\|^2 \\ & \quad + \omega_{\Delta a} \left\| \Delta a(t+k \mid t) \right\|^2), \\ s.t.\ :\ & v_{\min} \le v_h \le v_{\max}, \\ & a_{\min} \le a \le a_{\max}, \\ & (16), (18), \end{aligned} \tag{20}$$

where $v_{\min}$, $v_{\max}$ represent the boundaries of speed; $a_{\min}$, $a_{\max}$ are the boundaries of acceleration.

(2) Velocity planning for lane-keeping

When no feasible trajectory exists, the ego vehicle has to keep the current lane and decelerate to keep a safe distance from the leading car to wait for changing lane later rather than changing immediately. Thus, the ego vehicle enters the car-following model (CF). The vehicle kinematics for CF is discretized as

$$\begin{cases} \Delta ds(k+1) = \Delta ds(k) + \Delta v(k)\Delta t + t_h a_h(k)\Delta t, \\ \Delta v(k+1) = \Delta v(k) + (a_{\text{obs}}(k) - a_h(k))\Delta t, \end{cases} \tag{21}$$

where $\Delta ds(k) = ds(k) - S_d(k)$, $\Delta v(k) = v_h(k) - v_{\text{obs}}(k)$ denote the clearance error and speed error at time k; ds is the relative distance between the ego vehicle and the leading obstacle in the S-axis direction; a_h, a_{obs} represent the acceleration of the ego vehicle and leading obstacle; Δt represents the discretization time step. In consideration of driving safety, ride comfort, and actuator physical characteristics, the CF system is restricted by the constraint of eq. (22) during CF [37].

$$\begin{cases} a_{h\min} \le a_h \le a_{h\max}, \\ \Delta a_{h\min} \le \Delta a_h \le \Delta a_{h\max}, \\ \Delta ds_{\min} \le \Delta ds \le \Delta ds_{\max}, \\ \Delta v_{\min} \le \Delta v \le \Delta v_{\max}, \\ v_{\min} \le v_h \le v_{\max}, \\ \max\{TTC\,\Delta v, ds_s\} \le ds, \end{cases} \tag{22}$$

where TTC denotes the time to collision; ds_s is the safe distance in extreme situations; $a_{h\min}$, $a_{h\max}$, $\Delta a_{h\min}$, $\Delta a_{h\max}$, $\Delta ds_{\min}$, $\Delta ds_{\max}$, $\Delta v_{\min}$, $\Delta v_{\max}$ are the boundaries of related coefficients. Both the tracking error and the ego vehicle's acceleration increment are set as the optimization objectives here. In consideration of computation efficiency, optimization is transformed into a quadratic programming problem. By synthesizing eqs. (21) and (22), the velocity planning problem for lane-keeping is obtained.

$$\begin{aligned} \min\ J = & \sum_{i=1}^{N_{p1}}(\omega_{\Delta d} \left\| \Delta ds \right\|^2 + \omega_{\Delta v} \left\| \Delta v \right\|^2) \\ & + \sum_{i=1}^{Nc}(\omega_{\Delta a_h} \left\| \Delta a_h \right\|^2), \\ s.t.\ & \begin{cases} a_{h\min} + \varepsilon\Delta a_{uh\min} \le a_h \le a_{h\max} + \varepsilon\Delta a_{uh\min}, \\ \Delta a_{h\min} + \varepsilon\Delta a_{uuh\min} \le \Delta a_h \le \Delta a_{h\max} + \varepsilon\Delta a_{uuh\min}, \\ \Delta ds_{\min} + \varepsilon\Delta ds_{u\min} \le \Delta ds \le \Delta ds_{\max} + \varepsilon\Delta ds_{u\min}, \\ \Delta v_{\min} + \varepsilon\Delta v_{u\min} \le \Delta v \le \Delta v_{\max} + \varepsilon\Delta v_{u\min}, \\ v_{\min} \le v_h \le v_{\max}, \\ \max\{TTC\,\Delta v, ds_s\} \le ds, \end{cases} \end{aligned} \tag{23}$$

where N_{p1}, N_c denote the predictive step and the control step; $\omega_{\Delta d}$, $\omega_{\Delta v}$, $\omega_{\Delta ah}$ represent the weights of relative distance error, relative velocity error, and acceleration increment, respectively; $\Delta a_{uh\min}$, $\Delta a_{uh\max}$, $\Delta a_{uuh\min}$, $\Delta a_{uuh\max}$, $\Delta ds_{u\min}$, $\Delta ds_{u\max}$, $\Delta v_{u\min}$, and $\Delta v_{u\max}$ are the relaxation factors of the related coefficients; ε is the slack factor. Moreover, when the ego vehicle keeps the current lane without an existing TO, the ego vehicle should be driven as fast as possible to enhance traffic efficiency so that v_{obs} can be set as $v_{\max}$ and $d(k)$ should always be larger than $S_d(k)$.

3 Motion tracking control

The tracking controller is presented in this section. A planar 2DOF model is established for motion tracking control, first. Then, a preview PI-MPC coordinated controller is established.

3.1 2DOF vehicle dynamics model

The more complete the dynamics model is described, the higher the control accuracy enables to be achieved. However, the computational burden might be heavy if a competitive model is used in consideration of the nonlinearity and high fidelity of the vehicle. Therefore, a simplified bicycle model is adopted here, as shown in Figure 6. According to Newton's law, the bicycle model is expressed as follows:

$$\begin{cases} m(\dot{v}+ur)=F_{y_f}+F_{y_r}, \\ I_z\dot{r}=l_fF_{yf}-l_rF_{yr}, \\ \dot{\psi}=r, \\ \dot{X}=u\cos\psi-(v+l_fr)\sin\psi, \\ \dot{Y}=u\sin\psi+(v+l_fr)\cos\psi, \end{cases} \tag{24}$$

where m denotes the mass of the vehicle; I_z is the vehicle's momentum of inertia around its vertical axis; l_f and l_r represent the distance from the CG to the front and rear axles; X, Y, and ψ are the longitudinal and lateral position and heading angle of the vehicle in the global Cartesian coordinate; u, v, and r are the longitudinal velocity, lateral velocity, and the yaw rate of the CG in the vehicle coordinate; F_x is the total tire longitudinal force; F_{yf} and F_{yr} are the lateral tire force of the front and rear tires. The vehicle is a front steering system based on the small-angle assumption, and the lateral tire force can be linearized as

$$\begin{cases} F_{yf}=C_f\alpha_f, \\ F_{yr}=C_r\alpha_r, \end{cases} \tag{25}$$

where C_f and C_r are the cornering stiffness values of the front and rear tires; α_f, α_r are the slip angles of the front and rear tires, and they can be approximated as

$$\begin{cases} \alpha_f=\delta-\dfrac{v+l_fr}{u}, \\ \alpha_r=-\dfrac{v-l_rr}{u}, \end{cases} \tag{26}$$

where δ is the vehicle steering angle. By synthesizing eqs. (24)–(26), the bicycle model in the global Cartesian coordinate can be written in the form of a time-varying state-space equation as

$$\begin{aligned} \dot{\mathbf{x}}&=\mathbf{A}\mathbf{x}+\mathbf{B}\mathbf{u}, \\ \mathbf{y}&=\mathbf{C}\mathbf{x}, \end{aligned} \tag{27}$$

where $\mathbf{x}=[v, \psi, r, Y, X]$ is the state vector, $\mathbf{u}=[\delta]$ is the input vector, and $\mathbf{y}=[\psi, Y]$ is the output vector. $\mathbf{A}$, $\mathbf{B}$, $\mathbf{C}$ are the state matrix, input matrix, and output matrix, respectively.

3.2 Motion tracking strategy

In accordance with the reference information from the planning level, a preview PI controller and an MPC controller are adopted to track motions in the longitudinal and lateral directions, respectively. Thus, the path-following problem would be transformed into a coordinated control problem, and the structure of the coordinated controller is shown in Figure 7.

The controlled system is converted into a discrete state model through the Euler method [38]; thus, an optimal control problem can be obtained. Here, the control increment $\Delta\mathbf{u}(k)=\mathbf{u}(k)-\mathbf{u}(k-1)$ is introduced as optimization variables. Therefore, the objective function of the optimal control problem is stated as

$$\begin{aligned} J=&\sum_{k=1}^{N_p}\left\| y(t+k\mid t)-\mathbf{y}_{\text{ref}}(t+k\mid t)\right\|_{\mathbf{Q}}^2 \\ &+\sum_{k=1}^{N_c-1}\left\|\Delta\mathbf{u}(t+k\mid t)\right\|_{\mathbf{R}}^2, \end{aligned} \tag{28}$$

where $\mathbf{y}_{\text{ref}}=[\psi_{\text{ref}}, Y_{\text{ref}}]$ denotes the reference path from the motion planning, and $\mathbf{Q}$, $\mathbf{R}$ are the weight matrices. The first

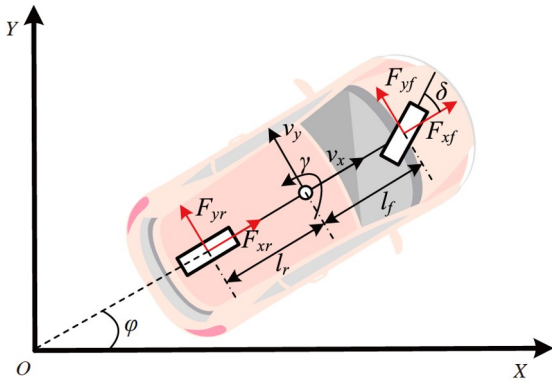

Figure 6 (Color online) Planar 2DOF model.

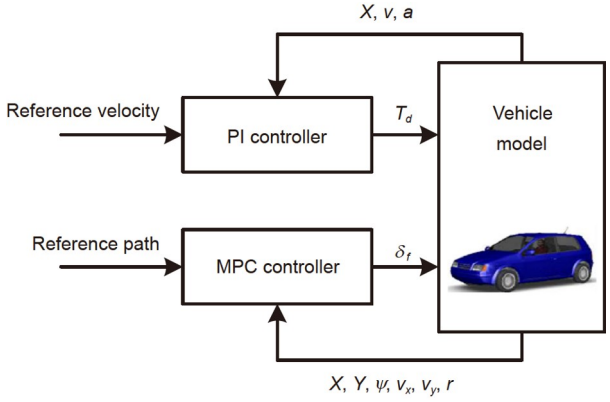

Figure 7 (Color online) Structure of coordinated controller.

part of eq. (28) decreases the tracking error, and the second one aims to penalize the variations of the input value. In other words, the function of the formulation is to guarantee that vehicles can follow a reference path as smoothly and quickly as possible. In addition, to improve tracking performance, some constraints must be imposed on the system. The constraints for output and input are written as

$$\begin{cases} Y_{\min} \le Y(k) \le Y_{\max}, \\ \psi_{\min} \le \psi(k) \le \psi_{\max}, \\ \mathbf{u}_{\min} \le \mathbf{u}(k) \le \mathbf{u}_{\max}, \\ \Delta\mathbf{u}_{\min} \le \Delta\mathbf{u}(k) \le \Delta\mathbf{u}_{\max}, \end{cases} \tag{29}$$

where $Y_{\min}$, $Y_{\max}$, $\psi_{\min}$, $\psi_{\max}$ are the boundaries of the constraints for the lateral position and heading angle; $\mathbf{u}_{\min}$, $\mathbf{u}_{\max}$, $\Delta\mathbf{u}_{\min}$, $\Delta\mathbf{u}_{\max}$ are the boundaries of the constraints for the input and its increment. Moreover, to ensure that a feasible solution exists during the online optimization process, the slack factor is adopted to soften constraints. By synthesizing eqs. (28) and (29), the problem is converted into a quadratic programming problem as follows:

$$\begin{aligned} \min\ J = & \sum_{k=1}^{N_p} \left\| \mathbf{y}(t+k \mid t) - \mathbf{y}_{\text{ref}}(t+k \mid t) \right\|_{\mathbf{Q}}^2 + \\ & \sum_{k=1}^{N_c-1} \left\| \Delta\mathbf{u}(t+k \mid t) \right\|_{\mathbf{R}}^2 + \rho\varepsilon^2, \\ s.t.\quad & Y_{\min} + \varepsilon v_{Y\min} \le Y(k) \le Y_{\max} + \varepsilon v_{Y\max}, \\ & \psi_{\min} + \varepsilon v_{\psi\min} \le \psi(k) \le \psi_{\max} + \varepsilon v_{\psi\max}, \\ & \mathbf{u}_{\min} \le \mathbf{u}(k) \le \mathbf{u}_{\max}, \\ & \Delta\mathbf{u}_{\min} \le \Delta\mathbf{u}(k) \le \Delta\mathbf{u}_{\max}, \\ & \varepsilon > 0, \end{aligned} \tag{30}$$

where ρ is the weight factor; $v_{Y\max}$, $v_{Y\min}$, $v_{\psi\max}$, and $v_{\psi\min}$ are the relaxation of the boundaries of the lateral position and heading angle. The sequence of the optimal input increments at the current cycle is obtained by solving the convex quadratic problem by SQP. The first element of sequences is adopted as the system input for the next cycle.

Additionally, the performance of path tracking is deeply affected by velocity tracking; therefore, the reference velocity profile must be also followed precisely. To guarantee the stable change of the velocity of the ego vehicle, the speed tracking problem is transformed into an acceleration tracking problem. The acceleration of an ego vehicle is assumed to be constant during a control step. Thus, on the basis of the kinematics law, the desired acceleration is obtained.

$$a_{\text{ref}} = \frac{v_{\text{ref}}^2 - v^2}{2L}, \tag{31}$$

where L is the preview distance, v_{ref} is the reference velocity of the preview point, and v is the velocity of the ego vehicle in the current cycle. In consideration of the change of vehicle system parameters and model mismatch, a PI controller is adopted to the closed-loop control of acceleration.

$$u_a = K_p(a_{\text{ref}} - a) + K_I(a_{\text{ref}} - a). \tag{32}$$

Subsequently, on the basis of the longitudinal dynamics model, the total driving/braking tire force can be obtained.

$$\begin{aligned} T_d = F_{xd}R = [mu_a + mg(\sin\alpha + f\cdot\cos\alpha) \\ + \frac{1}{2}\rho_{\text{air}} C_{\text{d}} A_{\text{wind}} v^2]R, \end{aligned} \tag{33}$$

where α is the road grade, f is the rolling resistance, ρ_{air} is the air massive density, and A_{wind} is the frontal area of the vehicle.

4 Results and discussion

Real traffic environments are dynamic and complex because they could be any combination of obstacles and road structures; thus, drivers must take different maneuvers to cope with different traffic scenarios. However, most maneuvers comprise several basic actions, including overtaking, lane-keeping, and car following. Therefore, several traffic scenarios are tested in this section through simulation to validate whether the proposed framework enables to carry out proper and correct driving maneuvers. The test scenarios are listed in Table 1. The first scenario is simple and aims to test the ability of the framework to avoid static obstacles. In this scenario, the ego vehicle should change lane if the adjacent lane is safe while an imminent collision exists in the current lane. The second scenario mainly tests the performance of the system in terms of car-following and lane-keeping, and the ego vehicle should decelerate or even stop to keep a safe distance from obstacles if it is not safe in both lanes. The ability of lane changing in dynamic traffic situations is tested in the third and fourth scenarios. The ego vehicle should follow the TO and keep its current lane if it is not safe to overtake, and it should change lane as soon as it is safe. The last scenario involves comparative tests, which aim to exhibit the advantages and superiorities of the proposed approach over the compared approach.

4.1 Simulation settings

A Carsim-Simulink joint platform is established to evaluate the performance of the controller proposed in this section. The vehicle system applied in the simulation is a four-wheel-motor drive electric model, and the vehicle model parameters are listed in Table 2. The desired total driving/braking force is averagely distributed to each wheel. The time steps of the planner and controller are 50 and 20 ms, respectively.

4.2 Simulation and analysis

In this section, different traffic scenarios, including car-following and avoidance of static and dynamic obstacles, are

Table 1 Tested traffic scenarios

Test scenarios	Description	Test abilities
Scenario 1	Lane change when there are static obstacles ahead	Lane-keeping, lane change
Scenario 2	Follow leading vehicle when there is not enough safe distance to change lane	Lane-keeping, car following
Scenarios 3 & 4	Lane change when there are moving obstacles ahead on a curved road	Lane-keeping, car following, lane change
Scenario 5 (Comparative)	Lane change when there are static/moving obstacles ahead on a straight road	Lane-keeping, car following, lane change

Table 2 Vehicle parameters

Symbol	Description	Value (Units)
m	Vehicle mass	1650 kg
l_f	Distance from CG to the front axle	1.400 m
l_r	Distance from CG to the rear axle	2.850 m
I_z	Yaw moment of inertia	3234 kg/m^2
R	Wheel effective radius	0.353 m

simulated to evaluate the performance of the proposed collision avoidance framework. In all traffic simulation result figures, the blue car-like symbol represents the ego vehicle, whereas the red and brown ones represent the obstacles in the right and left lanes, respectively. Moreover, the numbers in the symbols denote the different instants during the simulation; for instance, the blue symbol with number 1 is the initial instant of the ego vehicle.

(1) Scenario 1: This scenario is a continuous lane change maneuver in case of two static obstacles. The position and speed of the ego vehicle are [0, 2] and 70 km/h at the beginning of the simulation. The initial relative tangent distance between the obstacle in the right lane and the ego vehicle is 50 m, whereas another obstacle is 130 m. Figure 8 demonstrates the position information and the vehicle responses from Carsim of the whole process of collision avoidance. According to the figures, the ego vehicle almost moves at a constant speed during the whole simulation. Moreover, the ego vehicle is imposed to take maneuvers to change lane when approaching the leading obstacle and being affected by its PFs. Given that no other neighboring obstacles exist at the same time, the ego vehicle switches to the left and changes lane. After finishing the lane change maneuver, the ego vehicle moves along the left lane's centerline in consideration of the influence of the PFs of the road. When another front obstacle is encountered, another lane change behavior is performed.

(2) Scenario 2: This scenario involves car-following. The position and speed of the ego vehicle are [0, 2] and 70 km/h at the beginning of the simulation. The initial speed of both obstacles is 50 km/h. The initial relative tangent distance between the obstacle in the right lane and the ego vehicle is 50 m, whereas that of another obstacle is 35 m. Figure 9 demonstrates the position information and the vehicle responses from Carsim of the whole process of collision avoidance. The pictures show that the safe space on the ad-

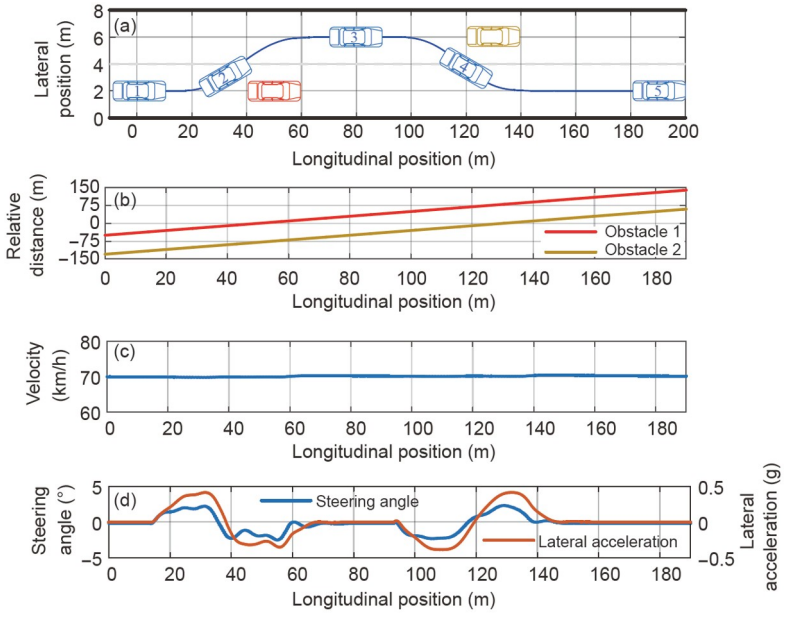

Figure 8 (Color online) Process of collision avoidance and dynamic response in scenario 1. (a) Paths of vehicles; (b) relative distance between the ego vehicle and the obstacles; (c) velocity; (d) steering angle and lateral acceleration.

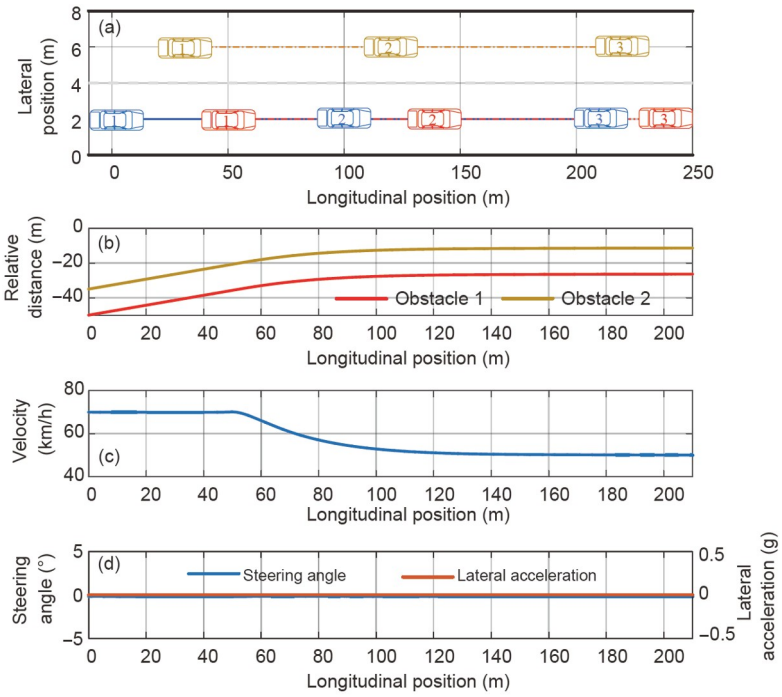

Figure 9 (Color online) Process of collision avoidance and dynamic responses in scenario 2. (a) Paths of vehicles; (b) relative distance between the ego vehicle and obstacles; (c) velocity; (d) steering angle and lateral acceleration.

jacent lane is not enough to change lane because of the existence of the neighboring obstacle. Thus, after deceleration, the ego vehicle moves with the same velocity as the leading vehicle to keep a safe distance from it instead of overtaking.

(3) Scenario 3: This scenario is a combination of the previous two scenarios. The initial position and speed of the ego vehicle are [0, 2] and 70 km/h. The initial speed of the obstacle in the right lane is 35 km/h, whereas that of the one in the left lane is 55 km/h. The corresponding relative tangent distances are 50 and 40 m. In addition, the obstacle in the left lane decelerates to 35 km/h from 55 km/h in 1.5 s during the period of overtaking. Figure 10 demonstrates the position information and the vehicle responses from Carsim of the whole process of collision avoidance. The figures show that the ego vehicle brakes to avoid collision when the safety distance is not enough for changing lane at first. After the obstacle in the left lane has driven far away, the ego vehicle begins to undertake a lane-change maneuver. However, the driving risk increases again during overtaking because of the deceleration of the brown obstacle. As for the adverse influence on traffic safety to change lane frequently between two lanes, the ego vehicle begins to slow down to keep the former maneuver. Eventually, the ego vehicle moves at 35 km/h and maintains a safe distance from the leading vehicle.

(4) Scenario 4: The initial position and speed of the ego vehicle are [0, 2] and 70 km/h. The initial speed of the obstacle in the right lane is 45 km/h, whereas that of the one in the left lane is 55 km/h. The corresponding relative tangent distances are 50 and 40 m. Figure 11 demonstrates the position information and the vehicle responses from Carsim of the whole process of collision avoidance. At the beginning of the simulation, the obstacle in the left lane is not far away from the ego vehicle. A collision may happen during the overtaking process; therefore, adjusting its velocity to follow the leading car at a safe distance and waiting for the obstacle on its left side to drive away is more secure. Once the safety distance constraint is met, the ego vehicle overtakes. When the second obstacle is encountered, other collision-free actions that resemble the ones to avoid the first obstacle are taken in order. Subsequently, the ego vehicle would accelerate to enhance traffic efficiency because no front obstacle exists after finishing the second lane change maneuver.

(5) Scenario 5 (comparative case study): To highlight the superiorities of our planning algorithm, a conventional planner in ref. [21] is introduced for comparison with our algorithm. Moreover, an optimal velocity planner serves the velocity profile for the path generated by the comparison algorithm. The optimal velocity planner is given as

$$\begin{aligned} &\min\ \rho_1\left(S(t_f)-S_f\right)^2+\int_0^{t_f}\left(\rho_2(v(t)-v_{\max}\right)^2+\rho_3 a(t)^2,\\ &s.t.\quad v_{\min}\le v(t)\le v_{\max},\\ &\quad a_{\min}\le a(t)\le a_{\max}, \end{aligned} \tag{34}$$

where ρ_1, ρ_2, ρ_3 are the weight factors; t_f is the travel time; S_f, $S(t_f)$ denote the length of the planned path and the travel distance, respectively.

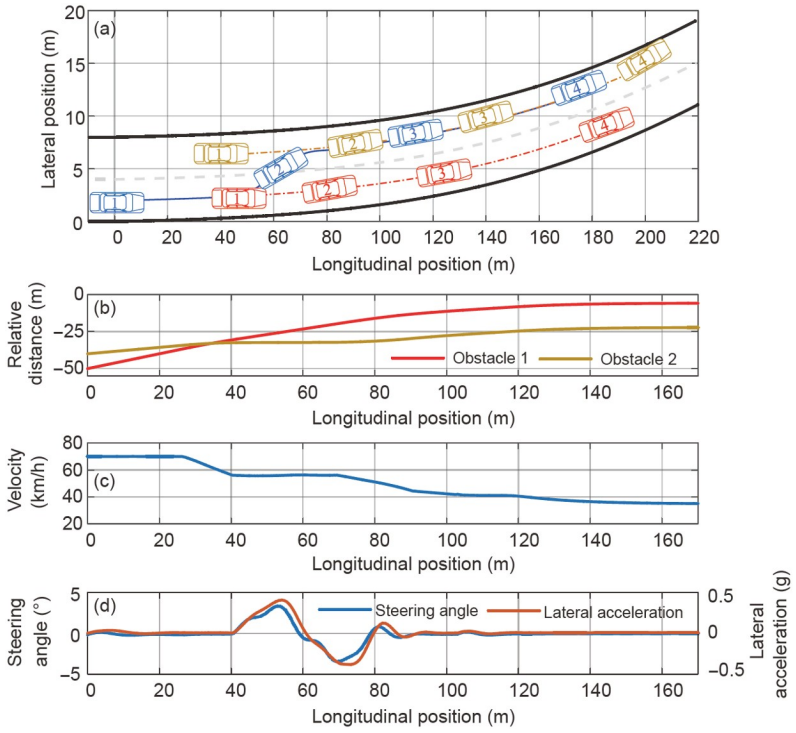

Figure 10 (Color online) Process of collision avoidance and dynamic responses in scenario 3. (a) Paths of vehicles; (b) relative distance between the ego vehicle and obstacles; (c) velocity; (d) steering angle and lateral acceleration.

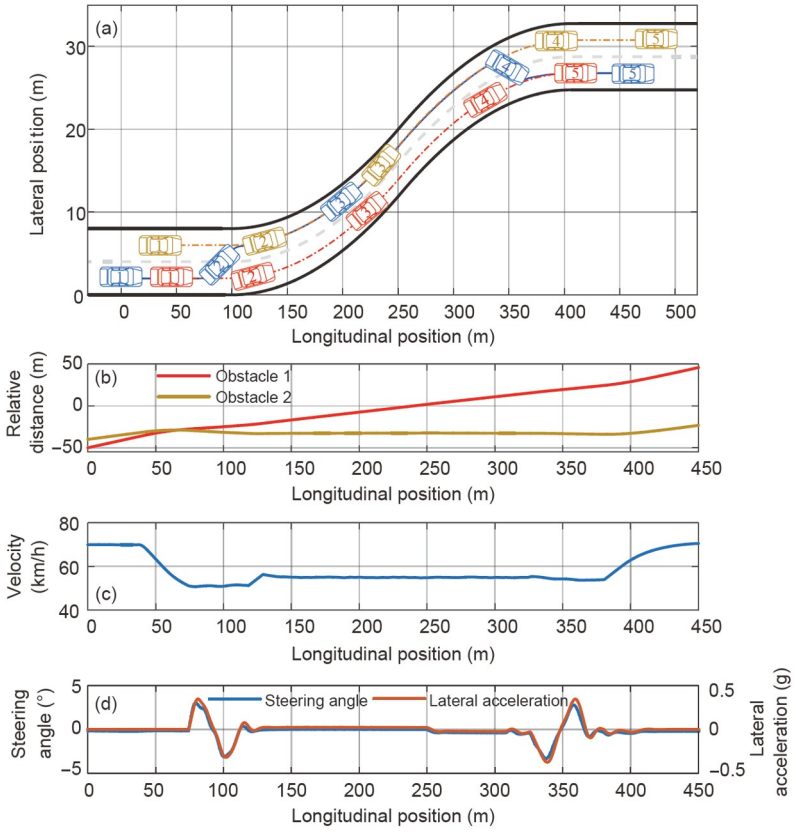

Figure 11 (Color online) Process of collision avoidance and dynamic responses in scenario 4. (a) Paths of vehicles; (b) relative distance between ego vehicle and obstacles; (c) velocity; (d) steering angle and lateral acceleration.

In the first comparative simulation test, the ego vehicle is supposed to avoid two preceding static obstacles that are initially 60 and 75 m from the front of the ego vehicle in the current lane. Figure 12 demonstrates the position information and speed change of the collision avoidance process in scenario 5.1. The results of the proposed method are shown by the solid lines, whereas the results of the standard method are denoted by the dash lines. According to Figure 12, the ego vehicles supervised by both approaches succeed in avoiding obstacles. Given the influence of the coupling potential energy distribution of the two obstacles, the ego vehicle controlled by the standard method tends to turn back to the right lane in the process of collision avoidance. These fluctuations are inconsistent with drivers' manipulations in real life and have adverse effects on ride comfort.

Another complex traffic scenario is tested to exhibit the advantages of the proposed approach further. Scenario 5.2 resembles scenario 4. The only difference between them is the road geometric that scenario 4 happens in the curved road, whereas scenario 5.2 is in a straight road. Figure 13 demonstrates the position information and speed change of the collision avoidance process. As shown in Figure 13, the collision avoidance process of the proposed algorithm is also similar to scenario 4. In the standard method, the planned path is trapped into the local minimum at the beginning of simulation due to the energy coupling of obstacles. Thus, the length of the planned path is short, leading to the ego vehicle decelerating rapidly to keep a safe distance from the front obstacle and wait to change lane later. When the obstacle on the adjacent lane passes approximately 80 m ahead, the ego vehicle just sets about to overtake, which looks too cautious. Moreover, the path for overtaking is not smooth, resulting in some unnecessary steering maneuvers. In summary, although the trajectory obtained by the standard method ensures driving security, it has poor ride comfort and traffic efficiencydue to existing rapid acceleration, unreasonable steering behavior, and conservative safe distance for lane change.

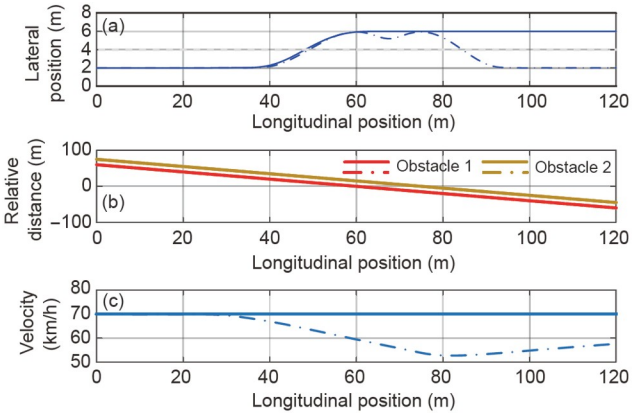

Figure 12 (Color online) Process of collision avoidance and speed change in scenario 5.1. (a) Paths of vehicles; (b) relative distance direction between the ego vehicle and obstacles; (c) velocity.

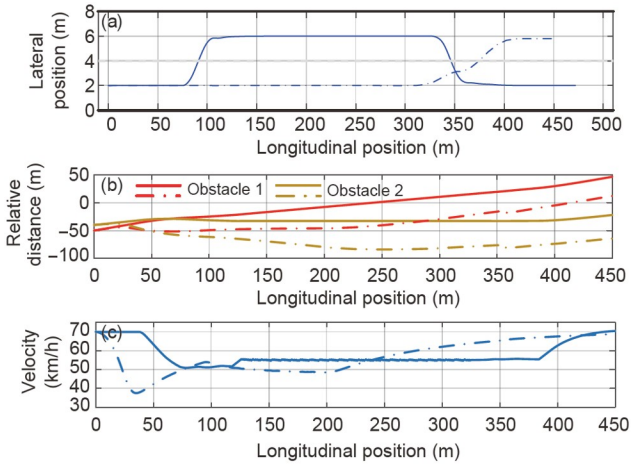

Figure 13 (Color online) Process of collision avoidance and speed change in scenario 5.2. (a) Paths of vehicles; (b) relative distance direction between ego vehicle and obstacles; (c) velocity.

5 Conclusions

This paper proposes a novel motion planning and tracking framework by leveraging improved APFs and a lane change strategy. Different traffic scenarios are tested to verify the effectiveness and merits of proposed algorithm. In accordance with the simulation results, some conclusions are drawn.

(1) The introduction of coordinate transformation and driving environment reconstruction enables hazard evaluation and motion planning to be conducted in the Frenet–Serret coordinate framework. Therefore, the algorithm can be utilized in different road geometric scenarios without any module modification, thus considerably improving the adaptability and applicability of the algorithm.

(2) Given the safety constraints in velocity planning, the ego vehicle would keep a safe distance from other obstacles, thereby ensuring dynamic safety during the lane change process.

(3) By hierarchically considering the effects of obstacles on driving safety, the proposed lane change strategy can not only perfectly address the problems of singularity and being trapped into the local minimum but also avoid the occurrence of huge step changes in planned paths for changing lane.

(4) As illustrated by the results, the proposed algorithm can enhance traffic efficiency and make the ego vehicle move smoothly during the collision avoidance process without sacrificing safety compared with the standard method.

This method assumes the absolutely reliable perception information, which is idealistic, whereas the information is mixed with noises and disturbances. Additionally, the path for changing lane is generated only on the basis of the potential energy distribution at the current moment, whereas the trajectory of obstacles in the future is not fully con-

sidered. As a result, collision avoidance maneuvers may become aggressive and conservative.

Thus, our future work will be focused on motion planning, which considers uncertain perception information and obstacle motion prediction.

This work was supported by the National Natural Science Foundation of China (Grant No. 51875061), the Technological Innovation and Application Development of Chongqing (Grant No. cstc2019jscx-zdztzxX0032), and the Graduate Scientific Research and Innovation Foundation of Chongqing, China (Grant No. CYB19063).

1 Wada T, Doi S, Tsuru N, et al. Characterization of expert drivers' last-second braking and its application to a collision avoidance system. IEEE Trans Intell Transp Syst, 2010, 11: 413–422
2 Ren Y, Zheng L, Yang W, et al. Potential field–based hierarchical adaptive cruise control for semi-autonomous electric vehicle. Proc Inst Mech Eng Part D-J Auto Eng, 2019, 233: 2479–2491
3 Graf Plessen M, Bernardini D, Esen H, et al. Spatial-based predictive control and geometric corridor planning for adaptive cruise control coupled with obstacle avoidance. IEEE Trans Contr Syst Technol, 2018, 26: 38–50
4 Dickmanns E D, Graefe V. Dynamic monocular machine vision. Machine Vis Apps, 1988, 1: 223–240
5 Vahidi A, Sciarretta A. Energy saving potentials of connected and automated vehicles. Transp Res Part C-Emerg Technol, 2018, 95: 822–843
6 Gonzalez D, Perez J, Milanes V, et al. A review of motion planning techniques for automated vehicles. IEEE Trans Intell Transp Syst, 2016, 17: 1135–1145
7 Bohren J, et al. Little ben: The ben franklin racing team's entry in the 2007 darpa urban challenge. J Field Robot, 2008, 25: 598–614
8 Bacha A, Bauman C, Faruque R, et al. Odin: Team victortango's entry in the darpa urban challenge. J Field Robot, 2008, 25: 467–492
9 Montemerlo M, Becker J, Bhat S, et al. Junior: The stanford entry in the urban challenge. J Field Robot, 2008, 25: 569–597
10 Kushleyev A, Likhachev M. Time-bounded lattice for efficient planning in dynamic environments. In: Proceedings of the 2009 IEEE International Conference on Robotics and Automation. IEEE, 2009. 4303–4309
11 Pivtoraiko M, Kelly A. Efficient constrained path planning via search in state lattices. In: Proceedings of International Symposium Artificial Intelligence Robotics & Automation in Space. Munich, 2005. 1–7
12 Kavraki L E, Svestka P, Latombe J C, et al. Probabilistic roadmaps for path planning in high-dimensional configuration spaces. IEEE Trans Robot Automat, 1996, 12: 566–580
13 LaValle S M, Kuffner Jr. J J. Randomized kinodynamic planning. Int J Robot Res, 2001, 20: 378–400
14 Brezak M, Petrovic I. Real-time approximation of clothoids with bounded error for path planning applications. IEEE Trans Robot, 2014, 30: 507–515
15 Perez J, Lattarulo R, Nashashibi F. Dynamic trajectory generation using continuous-curvature algorithms for door to door assistance vehicles. In: Proceedings of Intelligent Vehicle Symposium. IEEE, 2014. 510–515
16 Liang Z, Zheng G, Li J. Automatic parking path optimization based on bezier curve fitting. In: Proceedings of IEEE International Conference on Automation & Logistics. IEEE, 2012. 583–587
17 Berglund T, Brodnik A, Jonsson H, et al. Planning smooth and obstacle-avoiding b-spline paths for autonomous mining vehicles. IEEE Trans Automat Sci Eng, 2010, 7: 167–172
18 Piazzi A, Lo Bianco C G, Bertozzi M, et al. Quintic G/sup 2/-splines for the iterative steering of vision-based autonomous vehicles. IEEE Trans Intell Transp Syst, 2002, 3: 27–36
19 Ziegler J, Bender P, Schreiber M, et al. Making bertha drive—An autonomous journey on a historic route. IEEE Intell Transp Syst Mag, 2014, 6: 8–20
20 Song X, Cao H, Huang J. Vehicle path planning in various driving situations based on the elastic band theory for highway collision avoidance. Proc Inst Mech Eng Part D-J Autom Eng, 2013, 227: 1706–1722
21 Ji J, Khajepour A, Melek W W, et al. Path planning and tracking for vehicle collision avoidance based on model predictive control with multiconstraints. IEEE Trans Veh Technol, 2017, 66: 952–964
22 Hang P, Lv C, Huang C, et al. An integrated framework of decision making and motion planning for autonomous vehicles considering social behaviors. IEEE Trans Veh Technol, 2020, 69: 14458–14469
23 Li X, Xu S, Li S, et al. Simultaneous obstacle avoidance and target tracking of multiple wheeled mobile robots with certified safety. IEEE Trans Cybern, 2021, doi: 10.1109/TCYB.2021.3070385
24 Rasekhipour Y, Khajepour A, Chen S K, et al. A potential field-based model predictive path-planning controller for autonomous road vehicles. IEEE Trans Intell Transp Syst, 2017, 18: 1255–1267
25 Wang H, Huang Y, Khajepour A, et al. Crash mitigation in motion planning for autonomous vehicles. IEEE Trans Intell Transp Syst, 2019, 20: 3313–3323
26 Xu Z, Li S, Zhou X, et al. Dynamic neural networks for motion-force control of redundant manipulators: An optimization perspective. IEEE Trans Ind Electron, 2021, 68: 1525–1536
27 Han G, Fu W, Wang W, et al. The lateral tracking control for the intelligent vehicle based on adaptive PID neural network. Sensors, 2017, 17: 1244–1258
28 Wang Y, Ding H, Yuan J, et al. Output-feedback triple-step coordinated control for path following of autonomous ground vehicles. Mech Syst Signal Process, 2019, 116: 146–159
29 Ji X, Liu Y, He X, et al. Interactive control paradigm-based robust lateral stability controller design for autonomous automobile path tracking with uncertain disturbance: A dynamic game approach. IEEE Trans Veh Technol, 2018, 67: 6906–6920
30 Ren Y, Zheng L, Khajepour A. Integrated model predictive and torque vectoring control for path tracking of 4-wheel-driven autonomous vehicles. IET Intell Transp Syst, 2019, 13: 98–107
31 Guo H, Liu J, Cao D, et al. Dual-envelop-oriented moving horizon path tracking control for fully automated vehicles. Mechatronics, 2018, 50: 422–433
32 Barfoot T D, Clark C M. Motion planning for formations of mobile robots. Robotics Autonomous Syst, 2004, 46: 65–78
33 Hu X, Chen L, Tang B, et al. Dynamic path planning for autonomous driving on various roads with avoidance of static and moving obstacles. Mech Syst Signal Process, 2018, 100: 482–500
34 Wahid N, Zamzuri H, Rahman M, et al. Study on potential field based motion planning and control for automated vehicle collision avoidance systems. In: Proceedings of 2017 IEEE International conference on Mechatronics. IEEE, 2017. 208–213
35 Wang P, Gao S, Li L, et al. Obstacle avoidance path planning design for autonomous driving vehicles based on an improved artificial potential field algorithm. Energies, 2019, 12: 2342
36 Wang H, Kearney J, Atkinson K. Arc-length parameterized spline curves for real-time simulation. In: Proceedings of 5th International Conference on Curves and Surfaces (ICCS), 2002
37 Li S, Li K, Rajamani R, et al. Model predictive multi-objective vehicular adaptive cruise control. IEEE Trans Contr Syst Technol, 2011, 19: 556–566
38 Huang Y, Khajepour A, Zhu T, et al. A supervisory energy-saving controller for a novel anti-idling system of service vehicles. IEEE/ASME Trans Mechatron, 2017, 22: 1037–1046